HAL
open science

Current saturation and Coulomb interactions in organic single-crystal transistors

Simone Fratini, H. Xie, I. N. Hulea, S. Ciuchi, A. F. Morpurgo

To cite this version:

Simone Fratini, H. Xie, I. N. Hulea, S. Ciuchi, A. F. Morpurgo. Current saturation and Coulomb interactions in organic single-crystal transistors. New Journal of Physics, 2008, 10, pp.033031. 10.1088/1367-2630/10/3/033031 . hal-00704943

HAL Id: hal-00704943

https://hal.science/hal-00704943v1

Submitted on 6 Jun 2012

HAL is a multi-disciplinary open access archive for the deposit and dissemination of scientific research documents, whether they are published or not. The documents may come from teaching and research institutions in France or abroad, or from public or private research centers.

L'archive ouverte pluridisciplinaire **HAL**, est destinée au dépôt et à la diffusion de documents scientifiques de niveau recherche, publiés ou non, émanant des établissements d'enseignement et de recherche français ou étrangers, des laboratoires publics ou privés.

New Journal of Physics
The open-access journal for physics

Current saturation and Coulomb interactions in organic single-crystal transistors

S Fratini[1], H Xie[2], I N Hulea[2], S Ciuchi[3] and A F Morpurgo[2]

[1] Institut Néel—CNRS and Université Joseph Fourier, BP 166, F-38042 Grenoble Cedex 9, France
[2] Kavli Institute of Nanoscience, Delft University of Technology, Lorentzweg 1, 2628 CJ Delft, The Netherlands
[3] INFM-SMC, CNISM and Dipartimento di Fisica, Università dell'Aquila, via Vetoio, I-67010 Coppito-L'Aquila, Italy
E-mail: simone.fratini@grenoble.cnrs.fr

New Journal of Physics **10** (2008) 033031 (11pp)
Received 10 December 2007
Published 20 March 2008
Online at http://www.njp.org/
doi:10.1088/1367-2630/10/3/033031

Abstract. Electronic transport through rubrene single-crystal field-effect transistors (FETs) is investigated experimentally in the high carrier density regime ($n \simeq 0.1$ carrier molecule^{-1}). In this regime, we find that the current does not increase linearly with the density of charge carriers, and tends to saturate. At the same time, the activation energy for transport unexpectedly increases with increasing n. We perform a theoretical analysis in terms of a well-defined microscopic model for interacting Fröhlich polarons, which quantitatively accounts for our experimental observations. This work is particularly significant for our understanding of electronic transport through organic FETs.

Contents

1. Introduction 2
2. Experimental results 2
3. The microscopic model 4
4. Discussion 7
5. Conclusion 9
Acknowledgment 9
Appendix. Calculation of the polaron radius 9
References 10

© IOP Publishing Ltd and Deutsche Physikalische Gesellschaft

1. Introduction

The use of single-crystalline material for the fabrication of organic field-effect transistors (FETs) has given, over the past few years, the experimental control needed for the investigation of the intrinsic transport properties of dielectric/organic interfaces [1]. This has resulted in the observation of anisotropic transport [2], a metallic-like temperature dependence of the mobility [3], the Hall effect [4] and quasiparticle response in the infrared conductivity [5]. Following this progress, the successful quantitative analysis of experiments in terms of a simple microscopic model has recently been possible in single-crystal FETs with highly polarizable gate dielectrics [6]. In these devices, charge carriers accumulated electrostatically at the surface of the organic semiconductor were shown to interact strongly with the polarization in the dielectric, leading to the formation of Fröhlich polarons [7]. The quantitative agreement between the behavior predicted by the Fröhlich Hamiltonian and the experimental data demonstrates that the microscopic processes responsible for transport in organic FETs can be qualitatively different from that in bulk organic semiconductors.

Here, we investigate the transport properties of rubrene ($C_{42}H_{28}$) single-crystal FETs with highly polarizable Ta_2O_5 gate dielectrics, in the as yet unexplored high-carrier-density regime. We find that in this regime the electrical characteristics of the devices exhibit pronounced deviations from those of conventional FETs. Specifically, in all devices the source–drain current I_{sd} stops increasing linearly with the gate voltage V_g, and shows a clear saturation. Concomitantly, the activation energy for temperature-dependent transport increases when V_g increases, a trend opposite to that usually observed in organic transistors. We build on the Fröhlich model, which was used in our previous study to describe the dressing of the carriers by the polarizability of the gate dielectric [6], and find that the observed behavior can be quantitatively explained by considering the effects of the Coulomb interactions between holes. Our results confirm that organic single-crystal transistors are suitable for the experimental investigation of the intrinsic electronic properties of dielectric/organic interfaces, and extend our fundamental understanding of transport in organic transistors to the high-carrier-density regime.

2. Experimental results

The rubrene transistors used in our experiments are fabricated by laminating thin ($<1\,\mu$m thick) rubrene single crystals onto a substrate with pre-fabricated FET circuitry, as described in [8, 9]. The gate dielectric is a $\simeq$500 nm-thick layer of Ta_2O_5 (dielectric constant $\epsilon_s = 25$; breakdown voltage $\simeq$6.5 MV cm^{-1}), enabling the accumulation of up to 10^{14} holes cm^{-2} in the FET channel. During device operation, however, we never exceed gate voltage values corresponding to half the breakdown field, to minimize the chance of device failure [10] (we reach hole densities of 5×10^{13} cm^{-2}, i.e. one order of magnitude higher than in [6]). The transistor electrical characteristics were measured in the vacuum (10^{-6} mbar) chamber of a flow cryostat, between 300 and 125–210 K depending on the specific device (at low temperature the devices can easily break due to the difference in thermal expansion between crystal and substrate).

Figure 1 shows the source–drain current I_{sd} measured on two different devices as a function of gate voltage V_g, at different temperatures. Since the carrier density n in the channel is linearly proportional to the gate voltage V_g ($n = C(V_g - V_{th})/e$, where C is the capacitance per unit area

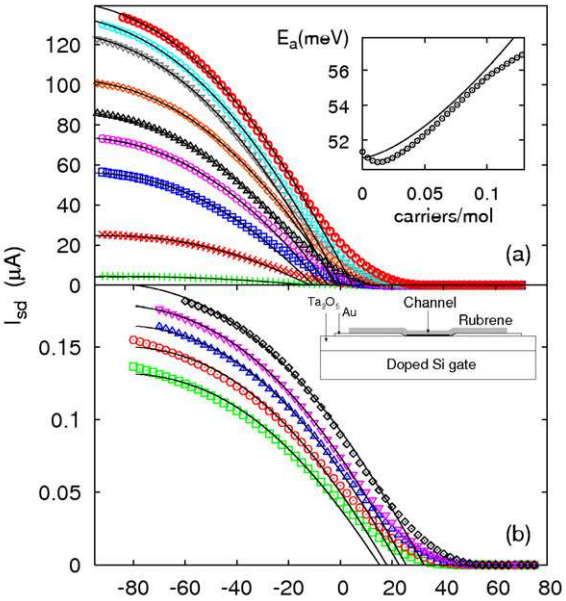

Figure 1. Source–drain current versus gate voltage measured for two different devices at different temperatures: (a) from top to bottom, $T = 280, 265, 250, 235, 215, 200, 175, 150$ and $125\,\mathrm{K}$ (measurements were performed at a source–drain bias $V_{sd} = -16\,\mathrm{V}$; the channel width and length are $W = 340\,\mu\mathrm{m}$ and $L = 200\,\mu\mathrm{m}$, respectively); (b) from top to bottom, $T = 300, 260, 240, 220$ and $210\,\mathrm{K}$ ($V_{sd} = -1\,\mathrm{V}$, $W = 28\,\mu\mathrm{m}$, $L = 630\,\mu\mathrm{m}$). The full lines are the theoretical fits. The inset in (a) shows the experimentally measured activation energy of I_{sd} plotted versus carrier density $n = C|V_g - V_{th}|/e$, compared with the theory (full line). The experimental error is comparable with the size of the data points. The device is sketched in (b).

and V_{th} is the threshold voltage), it is normally expected that I_{sd} also increases linearly with V_g. The data, however, show a pronounced deviation from the conventional linear behavior, since at high V_g the source–drain current tends to saturate. The effect is reversible and reproducible: the devices can be measured many times without noticeable difference in the data, which implies that the saturation of I_{sd} is not due to device degradation [10]. We have measured tens of similar devices (room-temperature mobility values between 1.0 and $1.5\,\mathrm{cm^2\,V\,s^{-1}}$) and found a similarly pronounced saturation of the source–drain current at high gate voltage in virtually all cases, albeit with some differences in the details of the I_{sd}–V_g characteristics (illustrated by the data in figures 1(a) and (b)).

The temperature dependence of the current I_{sd} is also unusual. At any fixed value of carrier density n, the current I_{sd} decreases in a thermally activated way [6]. The inset of figure 1(a) shows that the activation energy E_a depends on n and that, for densities larger than $\simeq 0.02$ holes molecule^{-1}, E_a *increases with increasing* n. This observation is surprising, because normally (e.g. in organic thin-film FETs) E_a exhibits the opposite trend, which is attributed to the effect of disorder (filling of traps) in the organic material.

A behavior of the I_{sd} versus V_g curves such as the one just described has not been reported earlier in FETs realized on other conventional gate dielectrics (e.g. SiO_2, Al_2O_3 and Si_3N_4). Only recently, a strongly nonlinear I_{sd}–V_g relation was observed in organic FETs with gate

electrolytes [11, 12]. Gate electrolytes enable the accumulation of a large density of carriers, 5×10^{13} carriers cm^{-2} or more, similar to our Ta_2O_5 dielectrics. At these densities, at which the charges accumulate in the uppermost molecular layer of the crystal [6], the average distance between the carriers is only a few molecules and the resulting (bare) Coulomb interaction is a few hundreds of millielectronvolts, much larger than the thermal energy at room temperature. This, together with the poor screening associated with the thermally activated motion of charge carriers, suggests that interactions may be responsible for the observed anomalous FET characteristics.

3. The microscopic model

As we proceed to show, the inclusion of Coulomb interactions between holes does indeed successfully account for our experimental findings. To introduce the theoretical framework needed for the quantitative description of the device characteristics, we recall the conclusions of [6], namely that holes in rubrene FETs with highly polarizable gate dielectrics form small Fröhlich polarons due to their strong interaction with the ionic polarization at the interface. This conclusion was established by analyzing transport measurements in the low-density regime, performed on FETs with a range of different gate dielectrics. Specifically, it was shown that, using gate dielectrics of increasing polarizability, the 'metallic-like' transport previously observed in rubrene [3, 13] is progressively suppressed, turning into an activated behavior characteristic of self-localized particles. The experimentally observed behavior was consistently explained in terms of the Fröhlich model—which describes the polar interaction with interface phonon modes—by including explicitly the narrow-band nature of the organic crystal [6]. In FETs with Ta_2O_5 devices, the most polarizable dielectric used in our previous work, the interaction with the interface modes completely dominates the carrier motion, reducing the mobility at 200 K by two orders of magnitude with respect to isolated rubrene.

Here, we extend the analysis of [6] to the high-density regime that had not been analyzed previously, by adding a term which accounts for the mutual Coulomb interactions between the carriers [14]. The resulting Hamiltonian:

$$H = -t \sum_{\langle ij \rangle} (c_i^+ c_j + c_j^+ c_i) + \frac{K}{2} \sum_{\ell} X_\ell^2 + \sum_{i,\ell} g_{i\ell} n_i X_\ell + \frac{1}{2} \sum_{i \neq j} n_i V_{ij} n_j, \tag{1}$$

is the simplest model that catches the main microscopic mechanisms that determine the transport in our devices: finite electronic bandwidth, polar coupling of the carriers with the gate dielectric and mutual interaction between carriers. The first three terms describe free holes in a tight-binding scheme (c_i^+ and c_i are the corresponding creation and annihilation operators on site i), interacting with lattice deformations X_ℓ through a non-local coupling $g_{i\ell}$. Physically, $g_{i\ell}$ represents the polar interaction between the holes in the two-dimensional (2D) conducting channel and the phonons at the organic/dielectric interface [6, 15]. When this interaction is sufficiently strong, as is the case for the rubrene/Ta_2O_5 interface, it leads to the formation of small polarons, i.e. self-trapped states whose characteristic radius is comparable with the lattice spacing. This is demonstrated theoretically in the appendix, and is confirmed by the experimental data, which exhibit a thermally activated mobility characteristic of small polarons (see [6] and figure 2 below). As in [6], we explicitly neglect the kinetic energy of the phonons, which is appropriate in the adiabatic regime, for which the lattice dynamics is slow compared to the band electrons.

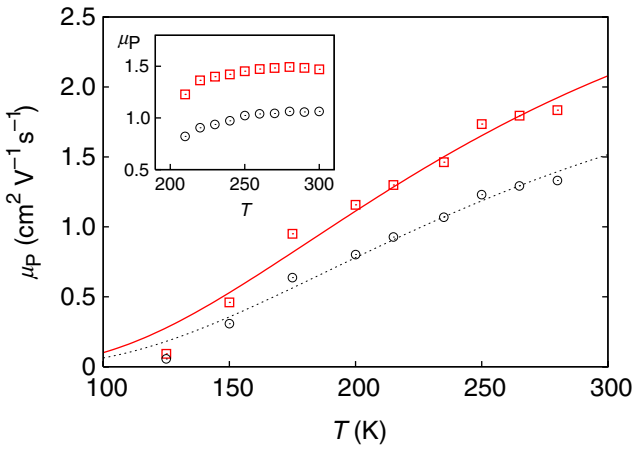

Figure 2. Polaron mobility extracted from the data of figure 1(a). Red squares are obtained by fitting the data with the theory for interacting polarons described in section 3, while black circles correspond to linear fits of the I_{sd}–V_g curves restricted to the low-density regime, as done in [6]. The lines are best fits to the polaronic thermally activated behavior, yielding respectively $\Delta = 53$ and 55 meV (see text). The inset is the polaron mobility for the sample of figure 1(b) (units are the same as in the main panel; the temperature range is too small to extract reliable values for Δ).

The last term—not considered previously—represents the mutual interaction between holes through the unscreened Coulomb repulsion V_{ij}, which is long-ranged (this contrasts with the Hubbard model, where a purely on-site interaction is considered, leading to the appearance of interaction effects only at densities close to 1 carrier molecule^{-1}). In the following, we evaluate quantitatively the effects of Coulomb interactions on the transport characteristics. We shall only present the main formulae needed for the comparison with the experiments, leaving the full details of the calculations to a further publication[4].

In the temperature range of the experiment the motion of small Fröhlich polarons at the rubrene/Ta_2O_5 interface takes place through successive uncorrelated hops from a given molecule to a nearest neighbor. In this case, the mobility can be rigorously determined by analyzing the hopping rate of a given carrier between two neighboring molecules (say $i = 1, 2$) [17]. Integrating out the electronic degrees of freedom, it is found that the hole dynamics is coupled to the long-range lattice polarization solely through the collective coordinate $Q = \frac{1}{g}\sum_\ell (g_{1\ell} - g_{2\ell}) X_\ell$. Taking advantage of the adiabatic assumption, we end up with the following

[4] It should be noted that the electron–lattice interaction in equation (1) can mediate an effective attraction between holes, leading under specific conditions to the stabilization of bipolarons, i.e. two holes bound together by a common lattice deformation. This requires in particular that the phonon-mediated attraction is sufficiently strong to overcome the instantaneous Coulomb repulsion between holes. This condition can be cast in terms of the effective dielectric constants of the interface at high and low frequencies, and corresponds to $\eta = (\epsilon_\infty + \kappa)/(\epsilon_s + \kappa)$ being less than a given critical value η_c. An accurate estimate $\eta_c = 0.131$ was given in [16] for a pure 2D Fröhlich interaction in the continuum limit. Such a critical value should be further reduced in the present case, because the finite distance z of the conducting channel to the interface suppresses the electron–phonon interaction at large momenta, $M_q \sim e^{-qz}/\sqrt{q}$ (see the appendix). For the present rubrene/Ta_2O_5 interface, we have $\eta = 0.26$, which lies safely above the critical value η_c, so that bipolaron formation can in principle be excluded.

double-well potential:

$$E_{\mathrm{ad}}(Q) = \frac{K}{4}Q^2 - \sqrt{\left(\frac{g}{2}Q - \frac{\xi}{2}\right)^2 + t^2}, \tag{2}$$

where we have defined $g^2 = \sum_\ell g_{1\ell}(g_{1\ell} - g_{2\ell})$. The physical meaning of the above equation is that in the adiabatic regime, the hole follows instantaneously the dynamics of the slow coordinate Q in the effective potential E_{ad}. The two minima at $Q \simeq \mp g/2\mathrm{K}$ are then associated with the hole being at sites 1 and 2, respectively. The corresponding hopping rate can be evaluated by standard techniques [18], by studying the escape rate of the coordinate Q over the barrier. The variable ξ that appears in equation (2) (defined below) accounts for the instantaneous repulsion of all the other carriers in the conducting layer, and vanishes in the low-density limit. In that case the double-well potential equation (2) is symmetric, with a barrier given by $\Delta = g^2/4K - t$ (the polaronic gap, valid in the strong coupling regime $g^2/4K \gg t$), all the carriers diffuse with the same hopping rate $w_0 = (\omega_{\mathrm{s}}/2\pi)\,\mathrm{e}^{-\Delta/k_{\mathrm{B}}T}$, and we recover the mobility of independent polarons obtained in [6], namely $\mu_{\mathrm{P}}(T) = (ea^2/\hbar T)w_0$ (here ω_{s} is the frequency of the interface optical phonons and a is the intermolecular distance).

In the high-density regime accessible with Ta_2O_5 gate dielectrics, it becomes essential to include the Coulomb interactions that were not analyzed previously, which requires considering the case of a finite ξ. From the model equation (1) it can be shown that:

$$\xi = \sum_{j\neq 1,2} (\bar{V}_{2j} - \bar{V}_{1j})n_j, \tag{3}$$

where $\bar{V}_{ij} = 2e^2/(\epsilon_{\mathrm{s}} + \kappa)/R_{ij}$ is the Coulomb potential, appropriately screened by the ionic polarization at the interface ($\kappa = 3$ is the dielectric constant of rubrene). A finite ξ causes an energy unbalance between the initial and final hopping sites (the double-well potential $E_{\mathrm{ad}}(Q)$ becomes asymmetric) so that the hopping rate changes to $w(\xi) = w_0\, e^{-\xi/2k_{\mathrm{B}}T}$. Now each carrier diffuses with a different hopping rate, determined by its own environment. Correspondingly, the mobility of the sample is obtained as the statistical average $\langle w(\xi)\rangle$ over all the possible values of the local electronic potential ξ.

Since the polaronic barrier sets the dominant energy scale, due to the high polarizability of the gate dielectric Ta_2O_5 used in our devices, we always have $\xi \ll \Delta$ in the explored density range. As a result, correlations between subsequent hops can be neglected to a first approximation, which corresponds to replacing $\langle w(\xi)\rangle \to w(\langle\xi\rangle)$. This yields the leading term of the mobility in the presence of electron–electron interactions as

$$\mu(T) = \mu_{\mathrm{P}}(T)\,\mathrm{e}^{-\langle\xi\rangle/2k_{\mathrm{B}}T}. \tag{4}$$

The density-dependent quantity $\langle\xi\rangle$ represents the average extra energy cost for hopping from site to site, induced by the long-range Coulomb interactions between the carriers. As the comparison between theory and experiments will show (see below), it is this dependence of μ on the density (through $\langle\xi\rangle$) that causes the saturation of I_{sd} observed in figure 1.

In the linear response regime, the calculation of $\langle\xi\rangle$ follows, through equation (3), from the statistical distribution of the occupation numbers $\{n_j\}$ *constrained* to $n_1 = 1$ (site 1 is initially occupied by the hole, which then hops to site 2). Such a constraint reflects the fact that the relaxation of the remaining carriers occurs on a timescale $\sim w_0^{-1}$, much longer than that of the hopping event under consideration, $\sim\omega_{\mathrm{s}}^{-1}$, and can be neglected. In this case, the occupation numbers $\{n_j\}$ are given, by definition, by the pair distribution function $g^{(2)}(R_{1j})$ of the electronic

system at equilibrium [19]. Furthermore, due to the diffusive nature of their hopping motion (transport is thermally activated), the small polarons behave as classical interacting particles. The two-body correlations of such a classical fluid of charged particles are determined solely by the Coulomb interactions, and are therefore equivalent to those of a classical 2D plasma. Observing that in the explored density range the mean interparticle distance is always larger than the lattice periodicity, we can use for $g^{(2)}$ the known pair distribution function of the 2D plasma in the continuous limit. Correspondingly, we can replace the discrete sum in equation (3) by an integral, which finally yields

$$\langle \xi \rangle = n \int \mathrm{d}\mathbf{r}\, [\bar{V}(\mathbf{r}+\mathbf{R}_{12}) - \bar{V}(\mathbf{r})]\, g^{(2)}(r) \equiv \frac{\pi}{2} n a^2 k_\mathrm{B} T F(\Gamma). \tag{5}$$

In the above equation, the universal function $F(\Gamma)$ is an intrinsic property of the 2D electron plasma. It depends on a single dimensionless parameter Γ that measures the ratio of the Coulomb interactions to the thermal energy. $F(\Gamma)$ can be evaluated directly by using the data of $g^{(2)}(r)$ available from extensive Monte Carlo simulations [20]. In the range $1 < \Gamma < 20$, we find $F(\Gamma) = 1 + 0.85\Gamma$ to within 1% accuracy. In the present FET geometry, the plasma interaction parameter is given by $\Gamma = 2\sqrt{\pi n} e^2/(k_\mathrm{B} T)/(\epsilon_\mathrm{s} + \kappa)$, and can attain the value $\sim$9 at the lowest temperatures/highest V_g, placing our devices in the range of weak to moderate interactions (electron crystallization is expected at $\Gamma = 125$).

4. Discussion

We are now in a position to compare the experimental data with our calculations. By inserting equation (5) into (4), and using the definition of Γ, we obtain the explicit functional dependence of the mobility μ on density $n = C(V_\mathrm{g}–V_\mathrm{th})/e$ and temperature. The I_sd–V_g curves can then be calculated from $I_\mathrm{sd} = A|V_\mathrm{g}–V_\mathrm{th}|\,\mathrm{e}^{-\langle\xi\rangle/2k_\mathrm{B}T}$, with $A = \mu_\mathrm{P} C V_\mathrm{sd} W/L$ having the dimensions of conductance (here W and L are the width and length of the channel, V_sd the applied source–drain voltage and e the electron charge). To analyze the data, we fix the temperature and fit the I_sd–V_g curve using μ_P and V_th as fitting parameters. The polaron microscopic parameters are obtained by analyzing the temperature dependence of μ_P extracted in this way.

The values of μ_P extracted for the different devices from the theory of interacting polarons are reported in figure 2 (red squares). They are close to the ones that one would obtain from linear fits of the I_sd–V_g curves in the low-density regime (the conventional definition of the mobility; data shown as black circles in figure 2) and they exhibit the same trend. Indeed, by comparing the temperature dependence of the fitted μ_P to the theoretical relation $\mu_\mathrm{P}(T) = (ea^2\omega_\mathrm{s}/2\pi k_\mathrm{B} T)\exp(-\Delta/k_\mathrm{B} T)$ we obtain, for the device of figure 1(a), the following values of the polaron parameters: $\omega_\mathrm{s}/(2\pi) = 390\,\mathrm{cm}^{-1}$ and $\Delta = 53\,\mathrm{meV}$. These values are comparable to those obtained by assuming a linear I_sd versus V_g dependence ($\omega_\mathrm{s}/(2\pi) = 315\,\mathrm{cm}^{-1}$ and $\Delta = 55\,\mathrm{meV}$). This shows that the results of the interpretation based on the theory with interactions is compatible with the analysis performed by only looking at the low-density part of the I_sd–V_g curves, and that the effect of the interactions is determined by the carrier density only (i.e. without the need to include any additional parameter). For the second device (the inset of figure 2), a precise quantitative analysis of the temperature dependence of the mobility is prevented by the restricted temperature range of the available data, and it is not possible to extract reliable values for the parameters $\omega_\mathrm{s}/(2\pi)$ and Δ. Still, the fitted values of μ_P and V_th are well defined for all the curves of figure 1(b), thus allowing for an accurate analysis of the density dependence of the mobility at each given temperature.

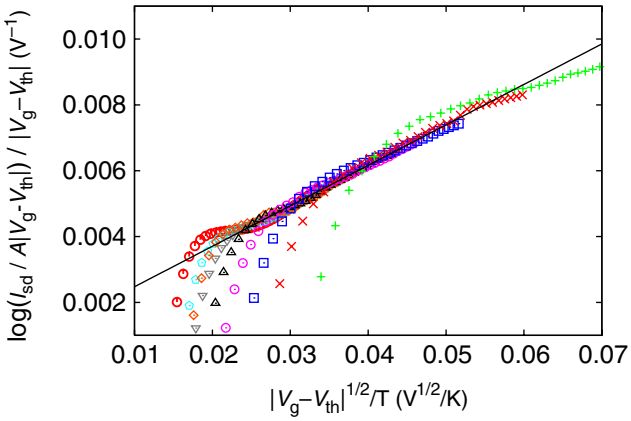

Figure 3. Scaling plot of the data of figure 1(a) (the same symbols have been used). The full line corresponds to the prediction of the 2D classical plasma.

The values of $V_{\rm th}$ obtained from the interacting theory also follow the same trend as those that one obtains by extrapolating the linear part of the $I_{\rm sd}$–$V_{\rm g}$ curves to zero current, i.e. the usual definition of $V_{\rm th}$. The two estimates differ by a systematic offset of $\sim$7 V, which is approximately the same for all samples and at all temperatures. Such a deviation does not have a particular physical significance, because the exact absolute value of $V_{\rm th}$ defined in the usual way does not have a precise physical meaning.

The continuous lines in figures 1(a) and (b) are the results of the theoretical fits of the $I_{\rm sd}$–$V_{\rm g}$ curves, using the theory for interacting polarons. The theory reproduces the saturation of the source–drain current at high carrier density and the quantitative agreement with the data is remarkable, at all temperatures and in both the devices analyzed. From equation (4), we see that theory predicts an activation energy which increases with increasing density (via the term $\langle\xi\rangle/2$). This is illustrated in the inset of figure 1(a), where the circles are the experimental values extracted from the data and the continuous line is the theoretical curve computed using equation (5), again without any new free parameters. Also here the agreement is very satisfactory, and at small n we recover the value given by the analysis of the linear regime in terms of non-interacting polarons [6].

Notably, the theoretical derivation presented above implies that the density-induced increase of the hopping activation barrier (cf equation (4)) is a scaling function of the parameter Γ of the interacting plasma. This scaling behavior is checked in figure 3, where we use the experimental data to directly plot the quantity $\log(I_{\rm sd}/A|V_{\rm g}-V_{\rm th}|)/|V_{\rm g}-V_{\rm th}|$, which is proportional to the universal function $F(\Gamma)$ (see equations (4) and (5)) versus $\sqrt{|V_{\rm g}-V_{\rm th}|}/T \propto \Gamma$. In terms of these variables and at sufficiently high gate voltages, the data do indeed tend to collapse on a single linear curve corresponding to $F(\Gamma) = 1 + 0.85\Gamma$ (full line in the figure). Considering the high sensitivity to details of such a scaling plot, the agreement between theory and experiment is satisfactory. It confirms the validity of the assumptions underlying our derivation, giving a strong indication that the anomalous behavior of the electrical characteristics observed at finite carrier concentrations is indeed due to the long-range Coulomb interactions between the carriers.

5. Conclusion

We have studied electronic transport through rubrene single-crystal FETs in the high-density regime and found new unexpected phenomena, such as a saturation of the current I_{sd} versus V_g and an increase of the activation energy with increasing density. The experimental data are accurately reproduced by a theoretical analysis based on interacting small Fröhlich polarons, which naturally extends previous studies in the low-density regime to include the effect of the long-range Coulomb repulsion between charge carriers. Remarkably, the quantitative description of the high-density regime does not require the introduction of any new parameter, as the effect of the interactions is fully determined by the (known) density of charge carriers. Our results demonstrate that, by devoting sufficient effort to control the experimental systems, single-crystal organic FETs do allow a detailed quantitative study of the intrinsic transport properties of organic FETs.

Acknowledgment

We thank R W I de Boer and N Iosad for experimental help and the NWO and Nanoned for financial support.

Appendix. Calculation of the polaron radius

The theoretical analysis developed in the text treats the charge carriers as small Fröhlich polarons, having dimensions comparable to the lattice spacing. To demonstrate that this is the case, in this appendix we evaluate the radius of the polarons that form at a rubrene/Ta_2O_5 interface. To this aim we solve the adiabatic model equation (1) variationally for a single hole in the HOMO band, and evaluate the polaron radius R_P as a function of the electron–phonon coupling strength. The calculations indeed show that R_P is of the order of the lattice spacing.

The electron–phonon interaction g_{ij} is obtained from the Fourier transform of the electron–phonon matrix element $M_q = M_0\, e^{-qz}/\sqrt{q}$ [6, 15]. Here, $M_0^2 = 2\pi\hbar\omega_s e^2\beta/S$, where S is the total surface of the device, and z is the distance of the conducting layer to the polar dielectric. The parameter $\beta = (\epsilon_s - \epsilon_\infty)/(\epsilon_s + \kappa)/(\epsilon_\infty + \kappa)$ is a combination of the known dielectric constants of the gate dielectric and of the organic semiconductor, which determines the strength of the electron–phonon coupling. In principle, the interaction g_{ij} defined above must be cut off at short distances to account for the discreteness of the rubrene lattice. A precise prescription to carry out this procedure will be reported elsewhere. For the present purposes it suffices to say that the overall behavior of the polaron radius does not depend on the particular choice of the short-distance cutoff.

As is customary for lattice models, we introduce the dimensionless electron–phonon coupling

$$\lambda = \frac{E_P}{D}, \tag{A.1}$$

defined as the energy of a fully localized polaron in units of the half bandwidth $D \propto t$. The energy E_P can be written in general as:

$$E_P = \frac{\sum_{R_i} g_{0i}^2}{\hbar\omega_s}, \tag{A.2}$$

Table A.1. Polaron radius in units of the lattice spacing a for different values of the dimensionless electron–phonon coupling λ.

λ	0.1	0.2	0.4	0.7	1.0	1.2	1.4	1.6	2
R_P/a	6.0	3.7	2.3	1.6	1.2	0.9	0.5	0.4	0.3

where the sum spans all the lattice sites R_i. The model is solved by taking the following Gaussian trial wavefunction:

$$\phi(R_i) = \frac{1}{\mathcal{N}^{1/2}} \exp(-\alpha^2 R_i^2/2) \tag{A.3}$$

where $\mathcal{N}$ is a normalization factor. The parameter α is obtained after minimization of the ground-state energy. The polaron radius is then given by

$$R_P = \left[\sum_{R_i} \phi^2(R_i) R_i^2 \right]^{1/2}, \tag{A.4}$$

which tends to $1/\alpha$ in the large polaron limit (small α, $R_P \gg a$). The results for R_P at different values of the electron–phonon coupling are summarized in table A.1. As expected, the polaron radius becomes comparable to the lattice spacing around $\lambda \sim 1$, i.e. when the polaron energy is of the order of the half bandwidth.

Performing the sum in equation (A.2) with the electron–phonon coupling parameters appropriate to our devices ($\beta = 0.1$ and $z = 2$ Å), we obtain $E_P = 170$ meV. The width of the HOMO band in the rubrene crystal has been evaluated through a semi-empirical *ab initio* calculation in [21] as $2D = 341$ meV. Such a value should be considered as an upper bound to the actual bandwidth, which was shown in [22] to be sizably reduced by the effects of molecular polarization. A further effective reduction of the bandwidth can arise from thermal fluctuations, as considered in [13]. From the above arguments and from the definition equation (A.1), we conclude that $\lambda > 1$, which, as can be seen from table A.1, corresponds to a small polaron.

References

[1] Gershenson M E, Podzorov V and Morpurgo A F 2006 *Rev. Mod. Phys.* **78** 973
[2] Sundar V C *et al* 2004 *Science* **303** 1644
[3] Podzorov V *et al* 2004 *Phys. Rev. Lett.* **93** 086602
[4] Podzorov V *et al* 2005 *Phys. Rev. Lett.* **95** 226601
[5] Fischer M *et al* 2006 *Appl. Phys. Lett.* **89** 182103
[6] Hulea I N *et al* 2006 *Nat. Mater.* **5** 982
[7] Kirova N and Bussac M N 2003 *Phys. Rev.* B **68** 235312
[8] de Boer R W I, Klapwijk T M and Morpurgo A F 2003 *Appl. Phys. Lett.* **83** 4345
[9] de Boer R W I *et al* 2004 *Phys. Status Solidi* a **201** 1302
[10] de Boer R W I *et al* 2005 *Appl. Phys. Lett.* **86** 032103
[11] Shimotani H *et al* 2006 *Appl. Phys. Lett.* **89** 203501
[12] Panzer M J and Frisbie C D 2007 *J. Am. Chem. Soc.* **29** 6599
[13] Troisi A and Orlandi G 2006 *Phys. Rev. Lett.* **96** 086601
[14] Fratini S and Quémerais P 2000 *Eur. Phys. J.* B **14** 99

[15] Sak J 1972 *Phys. Rev.* B **6** 3981
Mori N and Ando T 1989 *Phys. Rev.* B **40** 6175
[16] Verbist G, Smondyrev M A, Peeters F M and Devreese J T 1992 *Phys. Rev.* B **45** 5262
[17] Lang I G and Firsov Yu A 1968 *Sov. Phys. Solid State* **9** 2701
[18] Chandrasekhar S 1943 *Rev. Mod. Phys.* **15** 1
[19] Hansen J P and McDonald I R 1976 *Theory of Simple Liquids* (London: Academic)
[20] Totsuji H 1978 *Phys. Rev* A **17** 399
[21] da Silva Filho D A, Kim E-G and Brédas J-L 2005 *Adv. Mater.* **17** 1072
[22] Bussac M N, Picon J D and Zuppiroli L 2004 *Europhys. Lett.* **66** 392